© 2017. Published by The Company of Biologists Ltd | Development (2017) 144, 2663-2672 doi:10.1242/dev.149815

RESEARCH ARTICLE

Architectural protein Pita cooperates with dCTCF in organization of functional boundaries in Bithorax complex

Olga Kyrchanova[1,*], Nikolay Zolotarev[2,*], Vladic Mogila[3,*], Oksana Maksimenko[2], Paul Schedl[3,4,‡] and Pavel Georgiev[1,‡]

ABSTRACT

Boundaries in the Bithorax complex (BX-C) of *Drosophila* delimit autonomous regulatory domains that drive parasegment-specific expression of homeotic genes. BX-C boundaries have two crucial functions: they must block crosstalk between adjacent regulatory domains and at the same time facilitate boundary bypass. The C2H2 zinc-finger protein Pita binds to several BX-C boundaries, including *Fab-7* and *Mcp*. To study Pita functions, we have used a boundary replacement strategy by substituting modified DNAs for the *Fab-7* boundary, which is located between the *iab-6* and *iab-7* regulatory domains. Multimerized Pita sites block *iab-6*↔*iab-7* crosstalk but fail to support *iab-6* regulation of *Abd-B* (bypass). In the case of *Fab-7*, we used a novel sensitized background to show that the two Pita-binding sites contribute to its boundary function. Although *Mcp* is from BX-C, it does not function appropriately when substituted for *Fab-7*: it blocks crosstalk but does not support bypass. Mutation of the *Mcp* Pita site disrupts blocking activity and also eliminates dCTCF binding. In contrast, mutation of the *Mcp* dCTCF site does not affect Pita binding, and this mutant boundary retains partial function.

KEY WORDS: Insulator, Chromatin organization, Zinc-finger transcription factors, Protein-protein interactions, Architectural proteins

INTRODUCTION

Studies over the past few decades have substantially enhanced our understanding of chromosomal architecture in multicellular eukaryotes and have revealed an intimate connection between structure and function. High-resolution chromosome conformation capture techniques have shown that human, mouse and *Drosophila* chromosomes are partitioned into a series of loops called topologically associating domains (TADs) (Dixon et al., 2012; Sexton et al., 2012; Rao et al., 2014; Dekker and Mirny, 2016). Loop formation is driven largely by a special class of *cis*-acting elements called boundaries or insulators that pair with each other. These elements have binding sites for architectural proteins that mediate the boundary-boundary pairing interactions responsible for loop formation (Liang et al., 2014; Maksimenko and Georgiev, 2014; Bouwman and de Laat, 2015; Dekker and Mirny, 2016). In transgenic assays, boundaries can block regulatory interactions between enhancers/silencers and target genes; however, when appropriately arranged, boundaries can also bring distant regulatory elements in contact with promoters (Gohl et al., 2011; Chetverina et al., 2014; Kyrchanova and Georgiev, 2014; Matzat and Lei, 2014; Fujioka et al., 2016).

Although only one architectural DNA-binding protein, CTCF, has been as yet identified in mammals (Ali et al., 2016; Ghirlando and Felsenfeld, 2016; Merkenschlager and Nora, 2016), ongoing studies suggest that *Drosophila* probably has many architectural proteins (Maksimenko et al., 2015; Zolotarev et al., 2016a). This discrepancy likely reflects the relatively simple methods and assays that are available for studying boundaries/insulators in flies that are not readily feasible in higher eukaryotes. However, in spite of the experimental advantages offered by the fly model system, there is only a limited amount of information on the functional roles of architectural proteins in their native environment.

One context where it is readily possible to study the functioning of the endogenous fly boundaries is the *Drosophila* Bithorax complex. As is the case for the mammalian Hox gene complexes, many of the boundaries in the *Drosophila* Bithorax complex (BX-C) use a homolog of the mammalian CTCF protein, dCTCF (Moon et al., 2005; Holohan et al., 2007; Mohan et al., 2007; Perez-Lluch et al., 2008; Bonchuk et al., 2015; Magbanua et al., 2015). BX-C contains three homeotic genes, *Ultrabithorax* (*Ubx*), *abdominal-A* (*abd-A*) and *Abdominal-B* (*Abd-B*), which are responsible for specifying the parasegments (PS5 to PS13) that make up the posterior two-thirds of the fly segments (A) (Lewis, 1978; Kyrchanova et al., 2015; Maeda and Karch, 2015). Expression of each homeotic gene in the appropriate parasegment-specific pattern is controlled by a series of nine *cis*-regulatory domains, *abx/bx*, *bxd/pbx* and *iab-2* to *iab-9*. In order to properly specify segment identity, these regulatory domains must be able to function autonomously. Genetic and molecular studies have shown that each of these regulatory domains is bracketed by boundary elements (*Fab-3*, *Fab-4*, *Mcp*, *Fab-6*, *Fab-7*, *Fab-8* and *AB-I*; Fig. 1A) (Celniker et al., 1990; Gyurkovics et al., 1990; Galloni et al., 1993; Karch et al., 1994; Kyrchanova et al., 2008, 2011, 2016; McCall et al., 1994; Mihaly et al., 1997, 2006; Barges et al., 2000; Iampietro et al., 2010; Bender and Lucas, 2013; Bowman et al., 2014). BX-C boundaries have two important functions (Kyrchanova et al., 2015): one is to block crosstalk between adjacent regulatory domains; the other is bypass activity, i.e. enabling distal regulatory domains to bypass one or more intervening boundaries and contact their regulatory targets.

The most thoroughly characterized BX-C boundary, *Fab-7*, is located between *iab-6* and *iab-7* (Fig. 1A). *Fab-7* deletions fuse the

[1]Department of the Control of Genetic Processes, Institute of Gene Biology, Russian Academy of Sciences, Moscow 119334, Russia. [2]Group of Molecular Organization of Genome, Institute of Gene Biology, Russian Academy of Sciences, Moscow 119334, Russia. [3]Laboratory of Regulation of Gene Expression in Development, Institute of Gene Biology, Russian Academy of Sciences, Moscow 119334, Russia. [4]Department of Molecular Biology, Princeton University, Princeton, NJ 08544, USA.
*These authors contributed equally to this work

‡Authors for correspondence (pschedl@princeton.edu; georgiev_p@mail.ru)

O.K., 0000-0002-6249-0418; N.Z., 0000-0001-7917-2822; V.M., 0000-0003-2398-0331; O.M., 0000-0003-3502-0303; P.G., 0000-0002-6509-3194

Received 25 January 2017; Accepted 8 June 2017

Development (2017) 144, 2663-2672 doi:10.1242/dev.149815

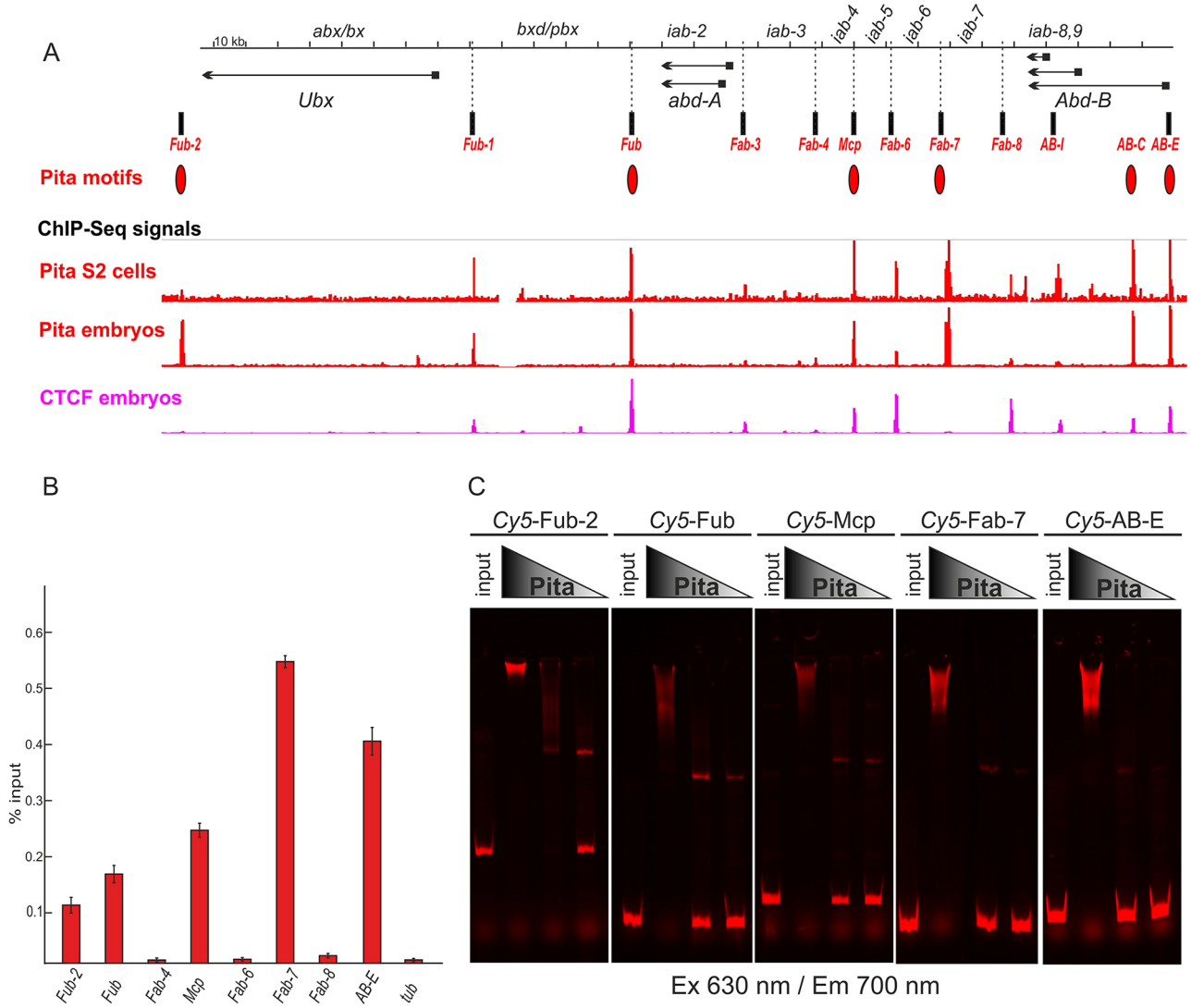

Fig. 1. Boundaries of the BX-C coincide with dCTCF and Pita. (A) Distribution of ChIP signals for Pita and dCTCF across the BX-C. The BX-C is presented as a sequence coordinate line. Transcripts of *Ubx*, *abd-A* and *Abd-B* are marked by horizontal arrows. The mapped insulator elements are indicated under the coordinate map as vertical black bars. Red ovals denote sequence motifs for Pita found in the BX-C. Tracks show the binding profiles for Pita and dCTCF according to the ChIP-Seq data. (B) Binding of Pita at the boundaries of BX-C. Chromatin was isolated from pupae and treated with antibodies against Pita. Nonspecific IgG was used as a negative control (not shown, see Fig. S1 for comparison). The results of ChIPs are presented as a percentage of input DNA. The *γTub37C* (tub)-coding region (devoid of binding sites for Pita) was used as a negative control. Error bars indicate standard deviations of the triplicate PCR measurements from two independent biological samples of chromatin. (C) EMSA of recombinant zinc-finger domains of Pita with the DNA fragments from BX-C containing Pita-binding sites (*Fub-2*, *Fub*, *Mcp*, *Fab-7* and *AB-E*). Zinc-finger domains of Pita fused with MBP were incubated with the Cy5-labeled DNA fragments. Specificity of the interaction was demonstrated by incubation of the DNA fragments with varying amounts of Pita protein, presented as a series of twofold dilutions. In parallel, the FAM-labeled DNA fragments with no binding sites for Pita were used as a negative control (data not shown).

iab-6 and *iab-7* regulatory domains, and mutant flies exhibit a complex mixture of gain- and loss-of-function phenotypes in PS11 (Gyurkovics et al., 1990; Karch et al., 1994; Mihaly et al., 1997). The gain-of-function phenotypes arise because the *iab-6* initiator inappropriately activates the *iab-7* domain in PS11 (A6), whereas the loss-of-function phenotypes arise because repressive elements in *iab-7* that are active in PS11 silence *iab-6* in that parasegment. Deletions that remove not only the *Fab-7* boundary, but also the *iab-7* Polycomb response element (PRE^{iab-7}) exhibit an exclusively gain-of-function transformation, and A6 is completely missing in mutant males. A similar fusion of neighboring regulatory domains and a consequent misregulation of *Abd-B* is observed when *Fab-6* and *Fab-8* are deleted (Barges et al., 2000; Iampietro et al., 2008, 2010).

Unlike other BX-C boundaries, *Fab-7* does not contain binding sites for dCTCF, and instead relies on other factors to confer boundary activity. Thus far, two developmentally regulated complexes have been shown to be important for *Fab-7* boundary function: Elba and LBC (Aoki et al., 2012; Wolle et al., 2015). The Elba complex confers boundary function during early embryogenesis, whereas LBC functions later in development. Although several different lines of evidence indicate that both of these factors must contribute to *Fab-7* activity, the boundary spans a DNA segment of over 1 kb and it is clear that other, partially redundant, factors are also important for boundary function (Wolle et al., 2015).

The studies reported here focus on a previously reported zinc-finger DNA-binding protein called Pita (Laundrie et al., 2003) or

Development (2017) 144, 2663-2672 doi:10.1242/dev.149815

Spotted Dick (Page et al., 2005) that has two binding sites in *Fab-7*. *pita* is an essential gene and null alleles die during larval stages. The mutant larvae exhibit a range of phenotypes, including an accumulation of abnormal mitotic figures in larval brains, severely reduced endoreplication in salivary glands, melanotic tumors and small imaginal discs. Experiments by Page et al. (2005) indicate that the mitotic and endoreplication defects arise because *pita* is required for DNA replication; however, this replication requirement is indirect, as Pita is present throughout the cell cycle and does not localize to replication foci. Instead, RNAi knockdown experiments in tissue culture cells suggest that Pita functions as a transcription activator, and argue that its role in replication is to ensure the expression of a specific origin of replication protein Orc4.

More recent work points to another very different function for *pita*, namely chromosomal architecture (Maksimenko et al., 2015). Chromatin immunoprecipitation (ChIP) experiments show that Pita binds to several boundaries in BX-C including *Fab-7* and *Mcp*. The Pita protein contains two recognizable domains: the N-terminal ZAD domain and a central cluster consisting of 10 C2H2 zinc-finger domains. Only part of the zinc-finger domains is responsible for DNA binding (Maksimenko et al., 2015). The N-terminal ZAD domain, together with an unstructured region located between the ZAD and zinc-finger domains, are thought to be involved in organizing long-distance interactions by the Pita protein (Zolotarev et al., 2016a,b). The ZAD domain is responsible for homodimer formation, whereas the unstructured region mediates interactions with the BTB domain of CP190. CP190 is a chromatin architectural protein that interacts with many DNA-binding proteins and is believed to promote loop formation by linking proteins bound to distant sequences (Vogelmann et al., 2014).

To better understand the role of Pita as a boundary factor and to elucidate how this activity might contribute to the regulation of BX-C homeotic gene expression, we have taken advantage of the *Fab-7*^{attP50} deletion (Wolle et al., 2015). The *attP* site in this allele can be used to introduce sequences of interest into *Fab-7*. Using this boundary replacement approach, we have explored the functioning of the Pita protein on its own and in the context of two previously characterized boundaries, *Fab-7* and *Mcp*. These experiments provide new insights into how boundaries impact BX-C gene regulation and segment specification.

RESULTS

Pita sites in the Bithorax complex

Previous genome-wide ChIP experiments with samples from embryos and S2 tissue culture cells identified several Pita-bound regions in BX-C with a high confidence (Maksimenko et al., 2015; Zolotarev et al., 2016a). These Pita-bound regions coincide with known functional elements in BX-C, including the *Fub-2*, *Fub*, *Mcp* and *Fab-7* boundaries, and the *Abd-B* [*AB-E*] and [*AB-C*] promoter regions (Fig. 1A and Fig. S1). Other known or suspected boundaries, *Fub-1*, *Fab-3*, *Fab-4*, *Fab-6* and *AB-I* also scored positive for Pita, but with a lower confidence. As shown in Fig. 1B, we found that ChIPs of chromatin, isolated from pupae, confirmed Pita binding to the high-confidence sites, but not to the other, lower confidence sites.

To further validate the identification of the Pita-binding sites in *Fub-2*, *Fub*, *Mcp*, *Fab-7* and *AB-E*, we tested for DNA binding *in vitro* using an electrophoretic mobility shift assay (EMSA) with fluorescently labeled DNA probes spanning the predicted Pita consensus-binding sites in each of these elements. For the Pita protein, we used an MBP fusion to the zinc-finger domain. As shown in Fig. 1C, the cluster of Pita zinc-finger domains fused with MBP binds to all five of these probes. To provide further evidence that Pita binds to the predicted consensus sequences and set the stage for functional studies, we mutated the Pita sites in the *Fab-7* and *Mcp* probes. As shown in Fig. S2, the fusion of the cluster of Pita zinc-finger domains with MBP shifts the wild-type probes for both *Fab-7* and *Mcp*, but not the probes in which the predicted Pita-binding sites are mutated.

Multimerized Pita-binding sites have blocking but not bypass activity

Next, we determined whether Pita has boundary activity on its own by replacing the *Fab-7* boundary with multimerized Pita-binding sites (*Pita*$^{\times 5}$). We used five Pita-binding sites because it was shown previously for Su(Hw), the best-studied insulator protein, that no fewer than four reiterated binding sites can display an enhancer-blocking activity in the transgenic assays (Scott et al., 1999). For replacement, we used the previously described *Fab-7*^{attP50} landing platform (Wolle et al., 2015). In this platform, the region spanning the *Fab-7* nuclease-hypersensitive sites, HS*, HS1 and HS2, and the hypersensitive site associated with the PRE^{iab-7}, HS3, are deleted and replaced with an *attP* target site for the *phiC31* recombination. The *attP* target site was used to insert a DNA fragment in which the Pita$^{\times 5}$ multimer was fused to the PRE^{iab-7} sequence (Fig. 2A). EMSA experiments show that Pita binds to the Pita$^{\times 5}$ *in vitro* (Fig. 2C). ChIP experiments confirm that the multimerized Pita-binding sites recruit Pita to the *Fab-7* region *in vivo*. Fig. 2B shows that Pita antibodies immunoprecipitate sequences from the very proximal end of the neighboring HS3 hypersensitive site (which corresponds to the PRE^{iab-7}). HS3 contains two GAGA factor (GAF) sites, and in the control experiments, GAF antibodies were found to immunoprecipitate the same sequence from the proximal end of HS3 (Schweinsberg et al., 2004).

We next examined the function of *Pita*$^{\times 5}$ in BX-C. In wild type, cells in A6 (PS11) and A7 (PS12) abdominal segments have different fates in adult males. The former establish distinct cuticular structures (tergites and sternites) and internal tissues of the A6 abdominal segment, whereas the latter are lost during morphogenesis. In *Fab-7*^{attP50} mutant males, *iab-7* is ectopically activated in all A6 (PS11) cells and they assume an A7 (PS12) identity. Consequently, these males lack both the A6 and A7 segments (Fig. 2D). Phenotypic analysis of the cuticle of adult male *Pita*$^{\times 5}$ flies indicates that the functioning of the multimerized Pita sites in the context of *Fab-7* resembles that seen for the multimerized *su(Hw)*- or *dCTCF*-binding sites (Kyrchanova et al., 2016). Just like these other multimers, *Pita*$^{\times 5}$ blocks crosstalk between *iab-6* and *iab-7*, but does not permit regulatory interactions between the distal *iab-6* regulatory domain and *Abd-B*. As a result, the cuticle in A6 resembles A5. In wild-type males, the A6 sternite has a distinct elongated banana shape and is devoid of bristles, whereas in A5 the sternite has a more compact quadrilateral shape and is covered in bristles. As can be seen in Fig. 2D, the A6 sternite in *Pita*$^{\times 5}$ males is compact and covered in bristles, just like the sternite in A5. A similar loss-of-function transformation is evident in the tergite. Whereas only the anterior and ventral edges of the A6 tergite have trichomes in wild-type flies, the A6 tergite in *Pita*$^{\times 5}$ males is completely covered in trichomes, just like A5.

Pita contributes to *Fab-7* boundary function

To further explore the functional properties of the Pita protein, we asked whether it contributes to the *Fab-7* boundary activity. The *Fab-7* boundary spans a DNA sequence of ~1.2 kb and contains

Development (2017) 144, 2663-2672 doi:10.1242/dev.149815

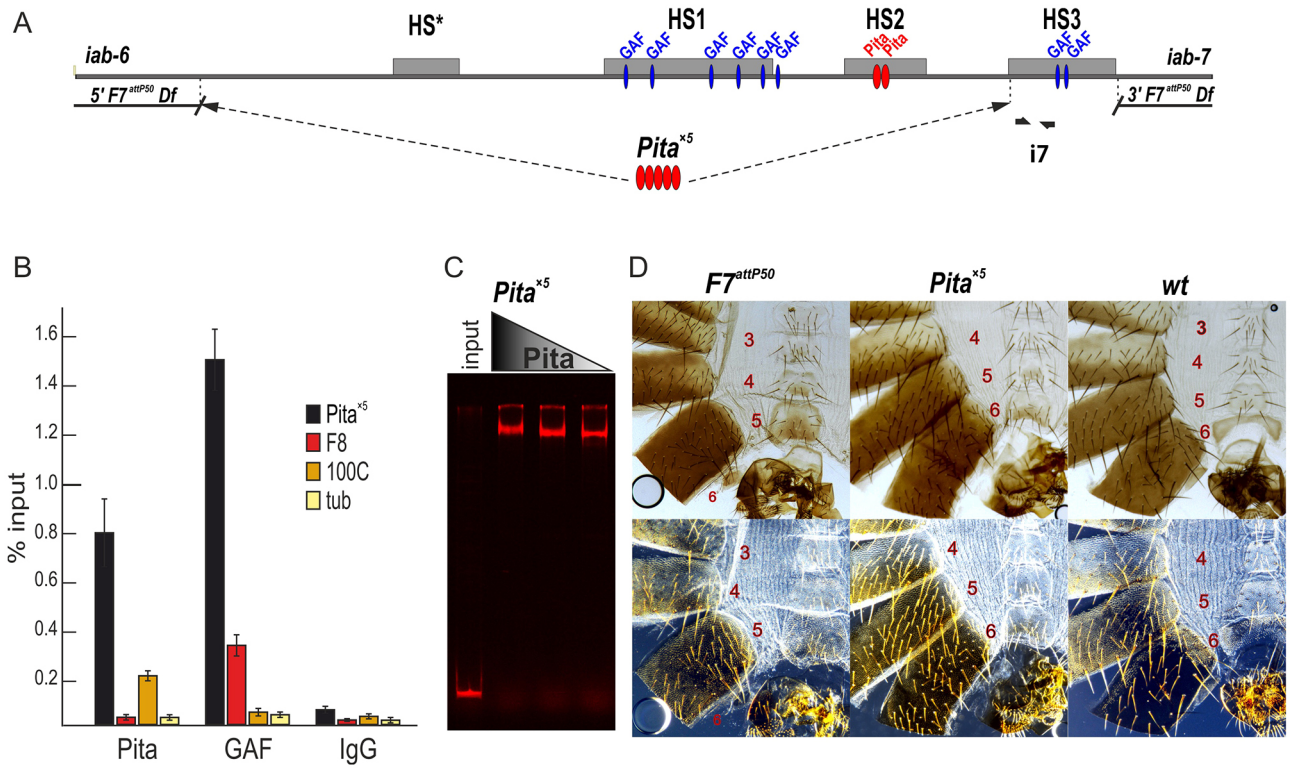

Fig. 2. The phenotypic effects of *Fab-7* replacement by multimerized Pita-binding sites. (A) A schematic presentation of the *Fab-7* boundary. Hypersensitive sites are shown as gray boxes. The proximal and distal deficiency endpoints of the $F7^{attP50}$ deletions are shown. GAF- and Pita-binding sites are designated as blue and red ovals, respectively. In this experiment, HS*, HS1 and HS2 are replaced by five Pita sites, whereas HS3 ($PRE^{iab\text{-}7}$) is retained. Bold black half-arrows (marked i7) indicate primers that were used for ChIP experiments. (B) Binding of Pita and GAF at the $Pita^{\times 5}$ fragment in $Pita^{\times 5}$ pupae. Nonspecific IgG was used as a negative control. The results of ChIP are presented as a percentage of input DNA. The *Fab-8* (F8) region was used as a positive control for GAF binding, the 100C region was used as a positive control for Pita binding. The γ*Tub37C*-coding region (tub), devoid of binding sites for Pita and GAF, was used as a negative control. Error bars indicate standard deviations of triplicate PCR measurements from two independent biological samples of chromatin. (C) EMSA of the recombinant zinc-finger domains of Pita with a $Pita^{\times 5}$ DNA fragment. Zinc-finger domains of Pita fused with MBP were incubated with a Cy5-labeled DNA fragment. In parallel, the FAM-labeled DNA fragment with no binding site for Pita was used as negative control (data not shown). (D) Morphology of the 4th to 6th male abdominal segments (numbered) is determined by the *Abd-B* cis-regulatory regions. $F7^{attP50}$ males have the classic gain-of-function transformation of A6 (PS11) into A7 (PS12) seen in mutations that remove both the *Fab-7* boundary and the $PRE^{iab\text{-}7}$, HS3. $Pita^{\times 5}$ demonstrates a strong loss-of-function phenotype: A6 sternite in males is quadrilateral and covered in bristles, just like the sternite in A5; whole A6 tergite is covered with trichomes, similar to the A5 tergite. Wild-type (*wt*) males have pigmented A5 and A6 tergites. The A6 sternite is recognizable by the absence of bristles and a specific form; A7 does not contribute to any visible cuticle structures. Trichomes are visible in the dark-field images (bottom row) and cover all the surface of A5 tergite, and only a thin stripe along the anterior and ventral edges of the A6 tergite.

three nuclease-hypersensitive sites: HS*, HS1 and HS2 (Fig. 3A). The *Fab-7* Pita-binding sites are located in the hypersensitive site HS2. Next to HS2 is HS3, which corresponds to the major PRE in the *iab-7* regulatory domain. Mutagenesis experiments, both in transgenes and in the context of BX-C, point to a considerable degree of redundancy in the *cis*-acting elements (Schweinsberg et al., 2004; Schweinsberg and Schedl, 2004; Wolle et al., 2015; Kyrchanova et al., 2016). Because of this redundancy, mutations in the binding sites for the factors that contribute to boundary activity can have little or no phenotypic effects. In this respect, *Fab-7* differs from the neighboring boundary, *Fab-8*, where mutations in the two dCTCF sites abrogate boundary activity (Moon et al., 2005; Kyrchanova et al., 2016). Because of this redundancy, we used two different contexts to test for Pita function. In the first, we introduced Pita mutations into a *Fab-7* replacement that includes HS1, HS2 and HS3. Although this replacement lacks HS*, it appears to be fully functional in an otherwise wild-type background. In the second, we introduced the Pita mutations into a *Fab-7* replacement that includes HS1 and HS2, but not HS3. As described further below, the removal of HS3 perturbs boundary function, giving a 'sensitized' background. As anticipated, redundancy compensates for the Pita mutations and we observed obvious phenotypic effects in only the sensitized *HS1+HS2* replacement.

For the *HS1+2+3* replacement series, ChIP experiments show that Pita is bound to the HS2 region in the wild-type version, whereas it is substantially reduced in the $HS1{+}2^{\Delta Pita}{+}3$ mutant (Fig. 3B). In spite of the loss of the Pita protein in the $HS1{+}2^{\Delta Pita}{+}3$ replacement, there was no detectable phenotypic effect, and like the starting *HS1+2+3* replacement, the mutant flies were phenotypically wild type (Fig. 3C). Thus, in this context the two Pita-binding sites are not needed for boundary function.

Very different results were obtained for the *HS1+2* replacement. The replacement itself has properties that have not been observed in any of the previously described *Fab-7* boundary mutations. First, the activity of the *HS1+2* replacement is differentially compromised in a rather striking tissue-specific pattern. As shown in the male *HS1+2* fly in Fig. 3C, the A6 sternite on the ventral side is completely absent, as would be expected for a gain-of-function transformation from PS11 (A6) to PS12 (A7) identity. Although the vast majority of *HS1+2* males lack an A6 sternite, infrequently (~10%) we observe a remaining small patch of sternite tissue (see Fig. S7). If a similar gain-of-function transformation occurred in the

Development (2017) 144, 2663-2672 doi:10.1242/dev.149815

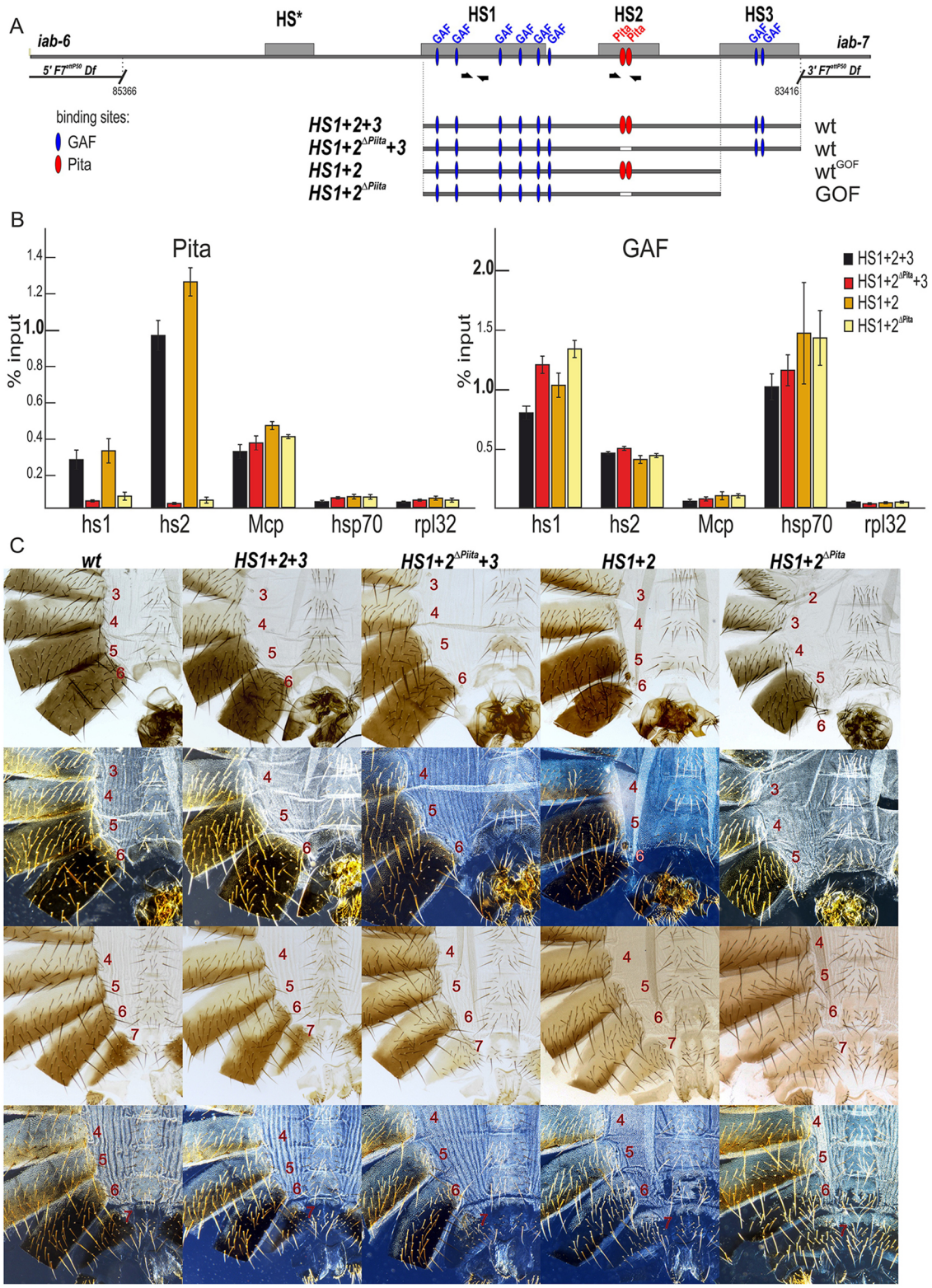

Fig. 3. Role of Pita-binding sites in *Fab-7* boundary function. (A) A schematic of the *Fab-7* boundary replacement constructs at the $F7^{attP50}$ site. Hypersensitive sites are shown as gray boxes. The proximal and distal deficiency endpoints of the $F7^{attP50}$ deletions are shown. GAF- and Pita-binding sites are designated as blue and red ovals, respectively. Bold black half-arrows (marked i7) indicate primers that were used for ChIP experiments. (B) Binding of Pita and GAF at the HS1 and HS2 regions in pupae of tested transgenic lines (*HS1+2+3*, *HS1+2*$^{\Delta Pita}$ *+3*, *HS1+2* and *HS1+2*$^{\Delta Pita}$). The results of ChIP are presented as a percentage of the input DNA. The *Mcp* region was used as a positive control for Pita binding, the *Hsp70* region was used as a positive control for GAF binding and the *RpL32*-coding region was used as a negative control for binding. Error bars indicate standard deviations of triplicate PCR measurements from two independent biological samples of chromatin. (C) All abdominal segments in *HS1+2+3* and *HS1+2*$^{\Delta Pita}$ *+3* males (first row, bright field; second row, dark field) and females (third row, bright field; fourth row, dark-field images) have essentially a wild-type identity. *HS1+2* males have a mixed wild-type and gain-of-function phenotype: an almost complete A6 tergite in combination with an absence of the A6 sternite. *HS1+2*$^{\Delta Pita}$ males and females have a strong gain-of-function phenotype with small spots of cells with loss-of-function features.

Development (2017) 144, 2663-2672 doi:10.1242/dev.149815

cells giving rise to the dorsal tergite, this tissue should also be absent in *HS1+2* males. However, as evident from Fig. 3C, all *HS1+2* males have an almost complete A6 tergite. Although there are often regions along the edges of the A6 tergite that are deformed or irregular, the tergite in the majority of the *HS1+2* males is close to the size of the A6 tergite in wild type and, judging from the unique pattern of trichomes in A6, is properly specified. A preferential reduction in boundary activity in the ventral tissues is also evident in female flies. Whereas the A6 tergite in the *HS1+2* females is properly specified and resembles that in wild type, this is not true for the sternite. Instead, the morphology of the A6 sternite indicates that there is a gain-of-function transformation in identity, albeit incomplete. Unlike wild type, the *HS1+2* A6 sternite has hairs pointing inward rather than outward, and has a partially abnormal inverted U-like shape. All of these morphological features are normally observed in A7, not in A6. It is worth noting that the specification of cell identity in A6 in *HS1+2* males and females differs from that observed in the standard *Fab-7* deletions. In standard deletions, A6 cells either activate *iab-7* and assume an A7 identity or silence A6 and assume and A5 identity. In contrast, in the *HS1+2* flies, the A6 cells either activate *iab-7* and assume an A7 identity or block *iab-6*↔*iab-7* crosstalk and assume the proper A6 identity. Second, all of the previously described *Fab-7* mutants are dominant, and their phenotypic effects are evident in flies that are heterozygous for the mutation. In contrast, the *HS1+HS2* replacement is recessive, and there are no detectable phenotypes in *HS1+HS2/+* flies.

ChIP experiments show that Pita is bound to the HS2 region in *HS1+2*, but not in the $HS1{+}2^{\Delta Pita}$ mutant (Fig. 3B). However, unlike the *HS1+2+3* series, loss of Pita binding in this already sensitized background leads to a further disruption of boundary function. Fig. 3C shows that $HS1{+}2^{\Delta Pita}$ males lack the entire A6 segment (both sternite and tergite) as would be expected for a complete transformation of PS11 into PS12. This is confirmed by the morphology of the A6 segment in $HS1{+}2^{\Delta Pita}$ females. A6 is transformed into a copy of A7. These findings indicate that Pita contributes to the boundary activity of *Fab-7*.

Pita is essential for blocking activity of the *Mcp* boundary

In previous studies, *Fab-7* has been replaced not only by multimerized binding sites for insulator proteins such as dCTCF, but also by the endogenous *D. melanogaster* boundary elements, *scs*, *gypsy su(Hw)* and *Fab-8* (Hogga et al., 2001; Kyrchanova et al., 2016). Of these three endogenous boundary elements, the only one that fully substitutes for *Fab-7* is the neighboring *Fab-8* boundary element (Kyrchanova et al., 2016). For this boundary element, rescuing activity is orientation dependent. When *Fab-8* is inserted in the same (forward) orientation, as the endogenous *Fab-8* boundary element, it rescues the $Fab\text{-}7^{attP50}$ deletion. It blocks crosstalk between *iab-6* and *iab-7* and is also able to facilitate boundary bypass. By contrast, when *Fab-8* is inserted in the reverse orientation, it still blocks crosstalk, but is no longer able to promote boundary bypass. *scs* inserted in both orientations resembles *Fab-8R* in that it blocks crosstalk and also prevents bypass. A similar result is observed for *gypsy su(Hw)* replacement in the epidermis; however, in the embryonic CNS, the *gypsy su(Hw)* replacement is inactive and fails to block *iab-6*↔*iab-7* crosstalk.

One interpretation of these findings is that BX-C boundaries have unique properties that enable them to prevent interactions between adjacent regulatory domains, but at the same time facilitate bypass (Kyrchanova et al., 2015). Supporting this idea, Iampietro et al. (2008) found that *Fab-7* could substitute for *Fab-8*. To test this hypothesis further and at the same time probe the functioning of the Pita protein, we selected the BX-C *Mcp* boundary, as it shares insulator proteins with both *Fab-7* and *Fab-8*. Like *Fab-7*, it has a Pita-binding site, and like *Fab-8*, it has a site for dCTCF (Fig. 4A). Although both sites are important for the *Mcp*-blocking activity in transgene assays (Kyrchanova et al., 2007), it is not known whether they are functional in the context of BX-C.

To explore these issues, we used the $Fab\text{-}7^{attP50}$ platform to introduce the 340 bp *Mcp* boundary either in the same, forward orientation (M^{340}) as it is in BX-C, or in the reverse orientation, fused with the $PRE^{iab\text{-}7}$ (Fig. 4A). The results for the forward orientation are shown in Fig. 4C. The same results were obtained for the reverse orientation (not shown).

Like the $Pita^{\times 5}$ replacement, M^{340} blocks crosstalk between *iab-6* and *iab-7* but does not permit boundary bypass. Whereas the gain-of-function transformation in $Fab\text{-}7^{attP50}$ deletion almost completely eliminates A6, this segment is restored in the *Mcp* replacement. However, instead of assuming an A6 (PS11) identity, the morphology of the cuticle in this segment is typical of the immediately anterior segment A5. In wild type, the A6 sternite has a banana shape and is devoid of bristles. In contrast, the A6 sternite in the male M^{340} fly, shown in Fig. 4C, resembles the sternite in A5: it has a quadrilateral shape and is covered in bristles. Similarly, the A6 tergite is completely covered in trichome hairs, just like the A5 tergite of wild type. Thus, unlike *Fab-8*, *Mcp* cannot substitute for *Fab-7*.

We next used *Mcp* fragments, which have either the Pita or dCTCF sites deleted, for the replacement experiments. Both mutations compromised the blocking activity of the *Mcp* replacement. The most straightforward is the deletion of the Pita site. As illustrated by the male fly in Fig. 4C, the $M^{340\Delta Pita}$ mutant boundary has a mixed gain-of-function and loss-of-function phenotype, like that observed in classical *Fab-7* boundary deletions that retain the $PRE^{iab\text{-}7}$, HS3. In the fly shown here, the A6 sternite is absent, whereas the size of the tergite is greatly reduced. These phenotypes are indicative of a gain-of-function transformation. Likewise, as expected for a loss-of-function transformation, the rudimentary tergite has trichome hairs distributed throughout, which is characteristic of A5.

Whereas a mixed gain-/loss-of-function phenotype (like that seen for $M^{340\Delta Pita}$) is expected for mutations that inactivate boundary function, this is not what was observed for $M^{340\Delta CTCF}$. Instead, the A6 (PS11) phenotypes in $M^{340\Delta CTCF}$ flies are a more complicated mixture of not only gain- and loss-of-function but also what appears to be wild type. A typical $M^{340\Delta CTCF}$ male fly is shown in Fig. 4C. Like most $M^{340\Delta Pita}$ males, the sternite is absent, as would be expected for a loss-of-function transformation of A6 (PS11) into A7 (PS12). However, in other respects it differs from the typical $M^{340\Delta Pita}$ male. Although the size of tergite is clearly reduced, it is larger than the residual tergite in most $M^{340\Delta Pita}$ males. In fact, as illustrated in Fig. S5, in about 10% of the $M^{340\Delta CTCF}$ males the size of A6 tergite is between one quarter and one half that of the wild-type A6 tergite. The other even more unusual feature is that the posterior side of the residual tergite is typically devoid of trichomes. As shown in the dark-field images in Fig. 4C and Fig. S5, this is most readily seen in $M^{340\Delta CTCF}$ males that have larger residual tergites. This morphological feature is characteristic of A6 (PS11), indicating that these cells have assumed a proper PS11 identity. However, it should be noted that there are also some males in which the residual tergite is covered in trichome hairs, indicating that the cells have assumed an A5 (PS10) identity. This is expected of the loss-of-function phenotype of boundary mutants. An equivalent

Development (2017) 144, 2663-2672 doi:10.1242/dev.149815

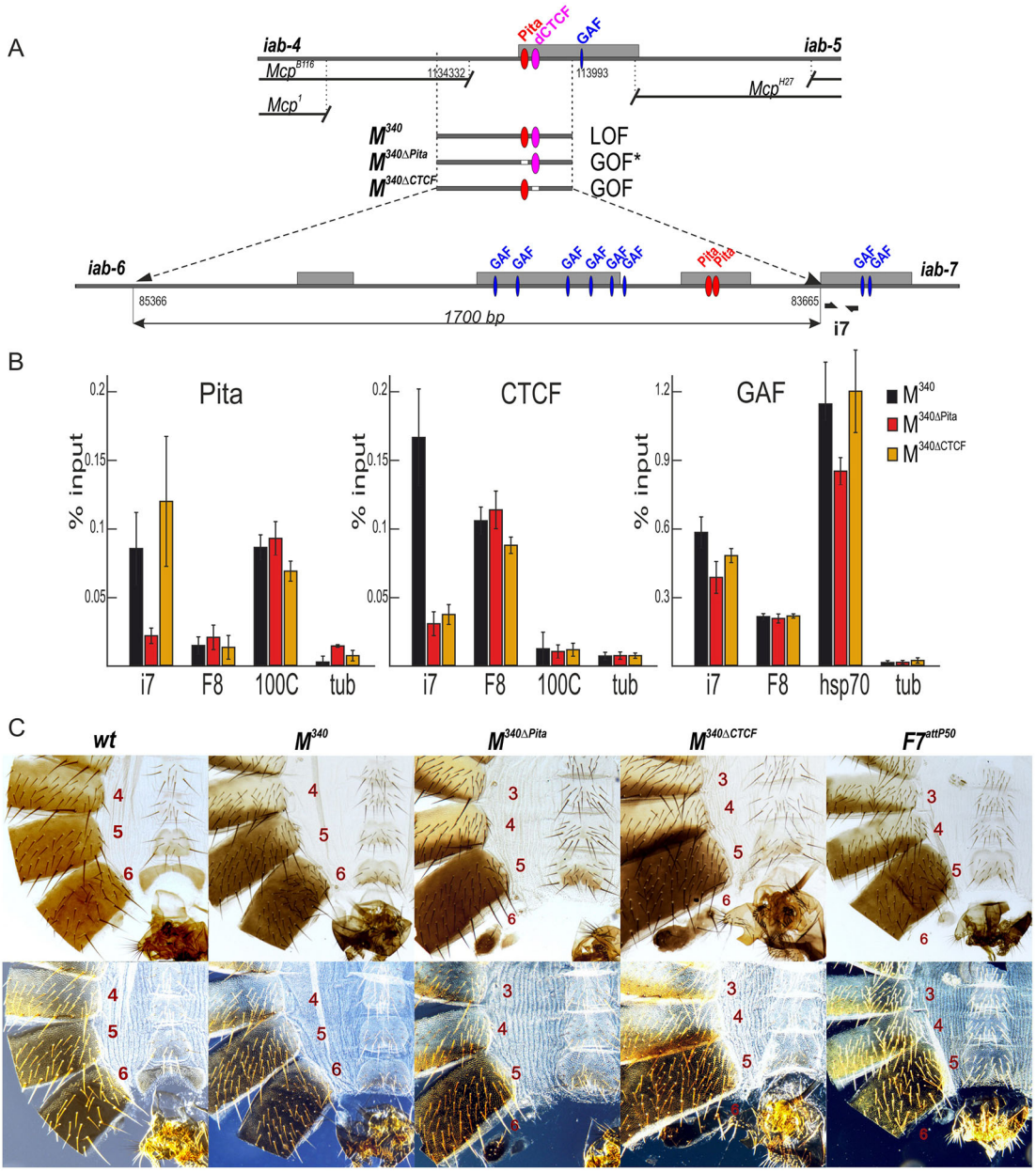

Fig. 4. Role of Pita- and CTCF-binding sites in *Mcp* insulator function. (A) Schematic of the *Mcp* boundary and replacement fragments used for the insertion at $F7^{attP50}$. The dCTCF-binding site is shown as magenta ovals. Bold black half-arrows (marked i7) below the map indicate primers that were used for ChIP experiments. Hypersensitive sites are shown as gray boxes. GAF- and Pita-binding sites are designated as blue and red ovals, respectively. (B) Binding of Pita, dCTCF and GAF at the $PRE^{iab\text{-}7}$ region in pupae of tested transgenic lines (*M340*, $M^{340\Delta Pita}$ and $M^{340\Delta CTCF}$). The results of ChIPs are presented as percentages of the input DNA. The 100C region was used as a positive control for Pita and hsp70 for GAF binding, the F8 region was used as a positive control for dCTCF and GAF binding, and the *γTub37C*-coding region was used as a negative control for binding. Error bars indicate standard deviations of triplicate PCR measurements from two independent biological samples of chromatin. (C) Morphology of the abdominal segments of the M^{340} mutant males (bright field, top row; dark field, bottom row). In M^{340} homozygous males, A6 is completely transformed into A5. The phenotypic effects are the same as in the case of $Pita^{\times 5}$. $M^{340\Delta Pita}$ and $M^{340\Delta CTCF}$ males demonstrate a mixed gain- and loss-of-function transformation of A6 segment. Phenotypes of M^{340} mutant females can be seen in Fig. S3.

loss-of-function phenotype can also be seen in the few males that have retained a residual sternite.

An important question is why does the deletion of the $M^{340\Delta CTCF}$ site lead to a mixture of gain- and loss-of-function, and wild-type phenotypes in A6, whereas the Pita site deletion gives the expected mixture of gain-/loss-of-function where the remnant cuticle is transformed to A5? One possible hint comes from ChIP experiments on the *Mcp* replacements M^{340}, $M^{340\Delta Pita}$ and $M^{340\Delta CTCF}$ (Fig. 4B). As expected, both Pita and dCTCF are present in ChIPs of the wild-type M^{340} replacement. However, the changes in Pita and dCTCF binding in the $M^{340\Delta Pita}$ and $M^{340\Delta CTCF}$ mutant replacements are not equivalent. For the $M^{340\Delta Pita}$, not only Pita but also dCTCF are reduced, indicating that dCTCF association is dependent on the presence of Pita. By contrast, for $M^{340\Delta CTCF}$, although the phenotype is unconventional, the effects of the mutation in the dCTCF site on protein association are completely conventional: dCTCF association is greatly reduced, while Pita binding is unaffected. Thus, one plausible explanation for the

Development (2017) 144, 2663-2672 doi:10.1242/dev.149815

distinct phenotypes of the $M^{340\Delta Pita}$ and $M^{340\Delta CTCF}$ would be the difference in protein association. In the case of $M^{340\Delta Pita}$, loss of both Pita and dCTCF would be equivalent to deleting the *Fab-7* boundary in terms of residual *Mcp* boundary activity. By contrast, in the $M^{340\Delta CTCF}$ mutant, Pita protein remains bound, and partial boundary function is retained. Significantly, as evidenced by the appropriately specified cuticle in A6, this partially functional *Mcp* boundary seems to have acquired bypass activity.

DISCUSSION

Previous studies on the Pita (also known as Spotted Dick) protein suggested that it is a transcriptional activator and showed that the replication defects in *pita* mutants and in RNAi knockdowns were due to a reduction in the expression of the replication origin protein Orc4 (Page et al., 2005). The experiments presented here, together with our previous studies (Maksimenko et al., 2015), indicate that *pita* has an additional, if not an entirely different, function, which is chromosome architecture. Below, we detail the evidence in favor of this conclusion, and also discuss the implications of our findings for boundary function in the context of BX-C.

Pita has 'classic' boundary activity

Our boundary replacement experiments provide compelling evidence that the zinc-finger protein Pita functions just like other insulator/architectural proteins. When placed in the context of *Fab-7*, multimerized Pita-binding sites block crosstalk between *iab-6* and *iab-7*, but are not permissive for the regulatory interactions between *iab-6* and the *Abd-B* gene. In this respect, the functioning of the multimerized Pita-binding sites is similar to that observed when multimerized sites for 'canonical' boundary factors, dCTCF and Su(Hw), are substituted for the *Fab-7* boundary. In the context of *Fab-7*, they also block crosstalk between *iab-6* and *iab-7*, but do not support bypass (Hogga et al., 2001; Kyrchanova et al., 2016).

Pita sites in HS2 contribute to Fab-7 boundary function

The boundary functions of the Pita protein are also supported by experiments testing its activity in a native context. For *Fab-7*, there are two Pita-binding sites in the HS2 hypersensitive region. Since previous studies have shown that HS1 is sufficient for full boundary activity, when the *iab-7* PRE (HS3) is present, it is clear that Pita function is redundant (Wolle et al., 2015). We confirmed this by introducing mutations in the two Pita-binding sites in a *Fab-7* boundary, *HS1+2+3*, that lacks the '*' nuclease-hypersensitive site, but contains the *iab-7* PRE. However, a different result was obtained in the context of a sensitized replacement, *HS1+2*, in which the *iab-7* PRE (HS3) is deleted. In this sensitized background, the two Pita-binding sites in HS2 are essential for boundary activity.

Interestingly, the sensitized *HS1+2 Fab-7* replacement has unprecedented properties. Unlike previously described *Fab-7* mutations, which are dominant, the boundary defects of *HS1+HS2* can be fully complemented by a wild-type boundary in *trans*. Additionally, as a homozygote, it has differential effects on the specification of dorsal and ventral tissues. The A6 (PS11) sternite is missing in *HS1+2* males. This gain-of-function transformation indicates that boundary activity is disrupted in the cells that give rise to this ventral cuticular structure. By contrast, the A6 tergite is not only nearly normal in size, but is also properly specified. This finding means that boundary activity is largely retained in the PS11 cells that give rise to dorsal cuticle structures.

It is also worth noting that *HS1+2* is very different from mutations that delete the *iab-7* PRE (HS3) but retain the *entire Fab-7* boundary (Mihaly et al., 1997). First, the vast majority of homozygous *iab-7* PRE (HS3) deletion males are indistinguishable from wild type, arguing that the HS3 deletion retains full boundary function. Second, in a few of the males (~2.5%), small sections of the dorsal A6 tergite are missing. This phenotype is most readily explained by a loss of PRE silencing, and consequent gain-of-function transformation, in a subset of the cells that give rise to the dorsal cuticle (Mihaly et al., 1997). As the *HS1+2* replacement differs from all of the *iab-7* PRE (HS3) deletions isolated by Mihaly et al. in that it lacks 'HS*', it would appear that this part of the boundary contains binding motifs for factors that are important for boundary function specifically in ventral tissues.

This would not be the only *Fab-7* boundary factor that has 'developmentally' restricted activity. The two large complexes known to be important for *Fab-7* HS1 boundary function, Elba and LBC, are active at different stages of development; the former in early embryos and the latter from mid-embryogenesis onwards. The fact that there is likely to be yet another boundary factor whose activity is developmentally restricted, fits with the idea that boundary function in flies can be subject to stage- and/or tissue-specific regulation (Magbanua et al., 2015).

The Mcp boundary, Pita and dCTCF

One of the paradoxes posed by the BX-C boundaries is that six of the nine regulatory domains in the complex are separated from their homeotic target genes by one or more boundaries. Consequently, these boundaries must, on the one hand, block regulatory interactions between adjacent domains and, on the other, facilitate boundary bypass. One of models to explain these two contradictory activities is that BX-C boundaries have unique properties, i.e. they are designed to block interactions between enhancers/silencers, but not between enhancers/silencers and promoters (Kyrchanova et al., 2015). This model gained currency from replacement experiments, which showed that the BX-C boundary *Fab-8* can substitute for *Fab-7*, while two heterologous boundaries cannot. A prediction of the model is that other BX-C boundaries could also substitute for *Fab-7*. However, contrary to this prediction, our experiments indicate that Mcp^{340} boundary behaves like the heterologous fly boundaries – it blocks both crosstalk and bypass.

Our analysis of the effects of mutations in the Pita and dCTCF sites of the Mcp^{340} boundary suggest that there is a complicated relationship between blocking crosstalk and blocking or enabling bypass. Although mutations in the Pita and dCTCF disrupt the functioning of Mcp^{340} replacement, the actual consequences of each mutation are quite distinct. In the case of the Pita mutation, we found that loss of Pita binding leads to a substantial reduction in the binding of dCTCF. This means that for this particular boundary, Pita association is required to recruit dCTCF. The requirement is not, however, reciprocal: deleting the *Mcp* dCTCF site has no effect on Pita association.

Correlated with the differential effects on protein binding, the $M^{340\Delta Pita}$ and $M^{340\Delta CTCF}$ mutants have quite different phenotypes. The phenotype (mixed gain and loss of function) of the former resembles a classic *Fab-7* boundary deletion in which the *iab-7* PRE (HS3) is retained (Mihaly et al., 1997). In contrast, the phenotype of the latter is a mixture of gain and loss of function, together with cuticle that has morphological features identical to that in A6 (PS11) of wild-type flies. The presence of cuticle that has the proper PS11 identity argues that $M^{340\Delta CTCF}$ retains residual boundary function that, in a subset of cells, is sufficient to not only block crosstalk between *iab-6* and *iab-7*, but is also able to facilitate *iab-6* bypass.

A simple interpretation of this finding is that the Pita protein differs from dCTCF in that it blocks crosstalk but can facilitate

Development (2017) 144, 2663-2672 doi:10.1242/dev.149815

bypass. However, this simple model is not supported by other findings. First, as noted above, just like multimerized dCTCF sites, multimerized Pita sites block both crosstalk and bypass when substituted for *Fab-7*. Second, the two Pita sites in *Fab-7* are not in themselves sufficient for blocking crosstalk. Third, the *Fab-8* boundary, which has two dCTCF sites, but no sites for Pita, has both blocking and bypass activity when substituted for *Fab-7* (Kyrchanova et al., 2016). Moreover, these dCTCF sites appear to contribute to the bypass activity of the *Fab-8* replacement. Thus, a more likely hypothesis is that there are other, as yet unidentified, factors that are bound to Mcp^{340} and contribute to the blocking and (newly acquired) bypass activities of the $M^{340\Delta CTCF}$ mutant, in addition to the Pita protein. Taken together with the finding that reversing *Fab-8* eliminates bypass activity (Kyrchanova et al., 2016), our experiments with *Mcp* suggest that there may not be a common mechanism for generating both blocking and bypass activity. Rather, each BX-C boundary would appear to deploy distinct mechanisms that are adapted for their specific context within the complex.

Is Pita also a transcriptional activator?

Based on their RNAi knockdown experiments in S2 cells, Page et al. (2005) suggested that Pita is a transcriptional activator and that it could play a crucial role in coordinating S phase progression. This idea was supported by their experiments showing that the replication defects induced by Pita depletion are caused by a reduction in *Orc4* expression. However, only 32 genes are downregulated (and 10 upregulated) after Pita RNAi, and most appear to have nothing to do with replication. Furthermore, as there are several thousand Pita sites in the genome, the number of affected genes is surprisingly low. In this light, an obvious question is whether blocking, instead of transcriptional activation, might account for the effects of Pita depletion on the *Orc4* transcription? Although we did not investigate how Pita functions in the S2 cells, there are reasons to think that this is a distinct possibility. ChIP experiments by Page et al. showed that Pita binds to a region upstream of the *Orc4* gene in S2 cells. ModEncode ChIP experiments indicate that there is a large PcG silenced domain just beyond this Pita site (Fig. S6). Thus, an alternative possibility is that *Orc4* expression is reduced when Pita is depleted, because the gene is silenced by the PcG spreading. Several of the other Pita transcriptional targets are also close to the PcG domains, and could be silenced in a similar manner (Fig. S6).

MATERIALS AND METHODS

Antibodies

Antibodies against Pita (amino acids 550-683), dCTCF (amino acids 612-818) and GAF (full length) were raised in rabbits and purified from the sera by the ammonium sulfate fractionation followed by affinity purification on the CNBr-activated Sepharose (GE Healthcare) according to standard protocols and have been previously described (Maksimenko et al., 2015).

Chromatin immunoprecipitation (ChIP)

Chromatin for the subsequent immunoprecipitations was prepared from 12-24 h embryos and mid-late pupae as described previously (Maksimenko et al., 2015). Aliquots of chromatin were incubated with rabbit antibodies against Pita (1:500), GAF (1:200) and dCTCF (1:500), or with nonspecific rabbit IgG (control). At least two independent biological replicates were made for each chromatin sample. The results of the ChIP experiments are presented as a percentage of the input genomic DNA after triplicate PCR measurements. The *RpL32*- or *γTub37C*-coding region (devoid of binding sites for the test proteins) was used as a negative control; Mcp, F8, 100C and hsp70 regions were used as positive controls. The sequences of used primers are presented in Table S1.

Electrophoretic mobility shift assays

Recombinant proteins for the binding assays were expressed and purified as described previously (Maksimenko et al., 2015). Fluorescently labeled DNA fragments were generated by PCR amplification with the corresponding FAM- or Cy5-labeled primers. Aliquots of purified recombinant proteins (10-15 µg) were incubated with the fluorescently labeled DNA fragments in the presence of nonspecific binding competitor poly(dI-dC). Incubations were performed in PBS (pH 8.0) containing 5 mM $MgCl_2$, 0.1 mM $ZnSO_4$, 1 mM DTT, 0.1% NP-40 and 10% glycerol at room temperature for 30 min. The mixtures were then resolved by nondenaturing 5% PAGE in 0.5× TBE buffer at 5 V/cm. Signals were detected using the Kodak Image System for the FAM-labeled fragments at Ex 500 nm/Em 535 nm and for the Cy5-labeled fragments at the Ex 630 nm/Em 700 nm.

Generation of the $Fab\text{-}7^{attP50}$ replacement lines

The strategy of the creation of the $Fab\text{-}7^{attP50}$ landing platform and generation of the *Fab-7* replacement lines is described in detail elsewhere (Wolle et al., 2015; Kyrchanova et al., 2016). DNA fragments used for the replacement experiments were generated by PCR amplification and verified by sequencing. The sequences of the used fragments are shown in Fig. S4.

Cuticle preparations

Adult abdominal cuticles of homozygous eclosed 3- to 4-day-old flies were prepared essentially as described previously (Kyrchanova et al., 2016) and mounted in Hoyer's solution. Photographs in the bright- or dark-field were taken on the Nikon SMZ18 stereomicroscope using Nikon DS-Ri2 digital camera, processed with ImageJ 1.50c4 and Fiji bundle 2.0.0-rc-46, and assembled using Impress of LibreOffice 5.2.3.3.

Acknowledgements

We are grateful to F. Karch for replacement constructs in the Fab-7 region.

Competing interests

The authors declare no competing or financial interests.

Author contributions

Conceptualization: O.K., P.S., P.G.; Methodology: O.K., N.Z., V.M., O.M., P.S., P.G.; Validation: O.K., N.Z., V.M., O.M.; Formal analysis: N.Z., O.M.; Investigation: O.K., N.Z., V.M., O.M., P.G.; Resources: P.S., P.G.; Data curation: N.Z., V.M., O.M.; Writing - original draft: O.K., P.S., P.G.; Writing - review & editing: O.K., V.M., P.S., P.G.; Visualization: O.K., N.Z., V.M., O.M.; Supervision: P.S., P.G.; Project administration: P.G.; Funding acquisition: P.S., P.G.

Funding

This study was supported by the Russian Science Foundation (project 14-24-00166 to P.G.), by a Ministry of Education and Science of the Russian Federation grant to the Institute of Gene Biology (14.B25.31.0 022 to P.S.) and by the National Institutes of Health (GM043432 to P.S.). Equipment belonging to the IGB RAS Shared Equipment Center, supported by the Ministry of Science and Education of the Russian Federation, was used in this study. Deposited in PMC for release after 12 months.

Supplementary information

Supplementary information available online at
http://dev.biologists.org/lookup/doi/10.1242/dev.149815.supplemental

References

Ali, T., Renkawitz, R. and Bartkuhn, M. (2016). Insulators and domains of gene expression. *Curr. Opin. Genet. Dev.* **37**, 17-26.

Aoki, T., Sarkeshik, A., Yates, J. and Schedl, P. (2012). Elba, a novel developmentally regulated chromatin boundary factor is a hetero-tripartite DNA binding complex. *Elife* **1**, e00171.

Barges, S., Mihaly, J., Galloni, M., Hagstrom, K., Muller, M., Shanower, G., Schedl, P., Gyurkovics, H. and Karch, F. (2000). The Fab-8 boundary defines the distal limit of the bithorax complex iab-7 domain and insulates iab-7 from initiation elements and a PRE in the adjacent iab-8 domain. *Development* **127**, 779-790.

Bender, W. and Lucas, M. (2013). The border between the ultrabithorax and abdominal-A regulatory domains in the Drosophila bithorax complex. *Genetics* **193**, 1135-1147.

Bonchuk, A., Maksimenko, O., Kyrchanova, O., Ivlieva, T., Mogila, V., Deshpande, G., Wolle, D., Schedl, P. and Georgiev, P. (2015). Functional

role of dimerization and CP190 interacting domains of CTCF protein in Drosophila melanogaster. *BMC Biol.* **13**, 163.

Bouwman, B. A. M. and de Laat, W. (2015). Architectural hallmarks of the pluripotent genome. *FEBS Lett.* **589**, 2905-2913.

Bowman, S. K., Deaton, A. M., Domingues, H., Wang, P. I., Sadreyev, R. I., Kingston, R. E. and Bender, W. (2014). H3K27 modifications define segmental regulatory domains in the Drosophila bithorax complex. *Elife* **3**, e02833.

Celniker, S. E., Sharma, S., Keelan, D. J. and Lewis, E. B. (1990). The molecular genetics of the bithorax complex of Drosophila: cis-regulation in the Abdominal-B domain. *EMBO J.* **9**, 4277-4286.

Chetverina, D., Aoki, T., Erokhin, M., Georgiev, P. and Schedl, P. (2014). Making connections: Insulators organize eukaryotic chromosomes into independent cis-regulatory networks. *BioEssays* **36**, 163-172.

Dekker, J. and Mirny, L. (2016). The 3D genome as moderator of chromosomal communication. *Cell* **164**, 1110-1121.

Dixon, J. R., Selvaraj, S., Yue, F., Kim, A., Li, Y., Shen, Y., Hu, M., Liu, J. S. and Ren, B. (2012). Topological domains in mammalian genomes identified by analysis of chromatin interactions. *Nature* **485**, 376-380.

Fujioka, M., Mistry, H., Schedl, P. and Jaynes, J. B. (2016). Determinants of Chromosome Architecture: Insulator Pairing in *cis* and in *trans*. *PLoS Genet.* **12**, e1005889.

Galloni, M., Gyurkovics, H., Schedl, P. and Karch, F. (1993). The bluetail transposon: evidence for independent cis-regulatory domains and domain boundaries in the bithorax complex. *EMBO J.* **12**, 1087-1097.

Ghirlando, R. and Felsenfeld, G. (2016). CTCF: making the right connections. *Genes Dev.* **30**, 881-891.

Gohl, D., Aoki, T., Blanton, J., Shanower, G., Kappes, G. and Schedl, P. (2011). Mechanism of chromosomal boundary action: roadblock, sink, or loop? *Genetics* **187**, 731-748.

Gyurkovics, H., Gausz, J., Kummer, J. and Karch, F. (1990). A new homeotic mutation in the Drosophila bithorax complex removes a boundary separating two domains of regulation. *EMBO J.* **9**, 2579-2585.

Hogga, I., Mihaly, J., Barges, S. and Karch, F. (2001). Replacement of Fab-7 by the gypsy or scs insulator disrupts long-distance regulatory interactions in the Abd-B gene of the bithorax complex. *Mol. Cell* **8**, 1145-1151.

Holohan, E. E., Kwong, C., Adryan, B., Bartkuhn, M., Herold, M., Renkawitz, R., Russell, S. and White, R. (2007). CTCF genomic binding sites in Drosophila and the organisation of the bithorax complex. *PLoS Genet.* **3**, e112.

Iampietro, C., Cleard, F., Gyurkovics, H., Maeda, R. K. and Karch, F. (2008). Boundary swapping in the Drosophila Bithorax complex. *Development* **135**, 3983-3987.

Iampietro, C., Gummalla, M., Mutero, A., Karch, F. and Maeda, R. K. (2010). Initiator elements function to determine the activity state of BX-C enhancers. *PLoS Genet.* **6**, e1001260.

Karch, F., Galloni, M., Sipos, L., Gausz, J., Gyurkovics, H. and Sched, P. (1994). Mcp and Fab-7: molecular analysis of putative boundaries of cis-regulatory domains in the bithorax complex of Drosophila melanogaster. *Nucleic Acids Res.* **22**, 3138-3146.

Kyrchanova, O. and Georgiev, P. (2014). Chromatin insulators and long-distance interactions in Drosophila. *FEBS Lett.* **588**, 8-14.

Kyrchanova, O., Toshchakov, S., Parshikov, A. and Georgiev, P. (2007). Study of the functional interaction between *Mcp* insulators from the *Drosophila* bithorax complex: effects of insulator pairing on enhancer-promoter communication. *Mol. Cell. Biol.* **27**, 3035-3043.

Kyrchanova, O., Toshchakov, S., Podstreshnaya, Y., Parshikov, A. and Georgiev, P. (2008). Functional interaction between the Fab-7 and Fab-8 boundaries and the upstream promoter region in the Drosophila Abd-B gene. *Mol. Cell. Biol.* **28**, 4188-4195.

Kyrchanova, O., Ivlieva, T., Toshchakov, S., Parshikov, A., Maksimenko, O. and Georgiev, P. (2011). Selective interactions of boundaries with upstream region of Abd-B promoter in Drosophila bithorax complex and role of dCTCF in this process. *Nucleic Acids Res.* **39**, 3042-3052.

Kyrchanova, O., Mogila, V., Wolle, D., Magbanua, J. P., White, R., Georgiev, P. and Schedl, P. (2015). The boundary paradox in the Bithorax complex. *Mech. Dev.* **138**, 122-132.

Kyrchanova, O., Mogila, V., Wolle, D., Deshpande, G., Parshikov, A., Cléard, F., Karch, F., Schedl, P. and Georgiev, P. (2016). Functional Dissection of the Blocking and Bypass Activities of the Fab-8 Boundary in the Drosophila Bithorax Complex. *PLoS Genet.* **12**, e1006188.

Laundrie, B., Peterson, J. S., Baum, J. S., Chang, J. C., Fileppo, D., Thompson, S. R. and McCall, K. (2003). Germline cell death is inhibited by P-element insertions disrupting the *dcp-1/pita* nested gene pair in Drosophila. *Genetics*. **165**, 1881-1888.

Lewis, E. B. (1978). A gene complex controlling segmentation in Drosophila. *Nature* **276**, 565-570.

Liang, J., Lacroix, L., Gamot, A., Cuddapah, S., Queille, S., Lhoumaud, P., Lepetit, P., Martin, P. G., Vogelmann, J., Court, F. et al. (2014). Chromatin immunoprecipitation indirect peaks highlight long-range interactions of insulator proteins and pol II pausing. *Mol. Cell*. **53**, 672-681.

Maeda, R. K. and Karch, F. (2015). The open for business model of the bithorax complex in Drosophila. *Chromosoma.* **124**, 293-307.

Magbanua, J. P., Runneburger, E., Russell, S. and White, R. (2015). A variably occupied CTCF binding site in the ultrabithorax gene in the Drosophila bithorax complex. *Mol. Cell. Biol.* **35**, 318-330.

Maksimenko, O. and Georgiev, P. (2014). Mechanisms and proteins involved in long-distance interactions. *Front Genet.* **5**, 28.

Maksimenko, O., Bartkuhn, M., Stakhov, V., Herold, M., Zolotarev, N., Jox, T., Buxa, M. K., Kirsch, R., Bonchuk, A., Fedotova, A. et al. (2015). Two new insulator proteins, Pita and ZIPIC, target CP190 to chromatin. *Genome Res.* **25**, 89-99.

Matzat, L. H. and Lei, E. P. (2014). Surviving an identity crisis: a revised view of chromatin insulators in the genomics era. *Biochim. Biophys. Acta* **1839**, 203-214.

McCall, K., O'Connor, M. B. and Bender, W. (1994). Enhancer traps in the Drosophila bithorax complex mark parasegmental domains. *Genetics* **138**, 387-399.

Merkenschlager, M. and Nora, E. P. (2016). CTCF and Cohesin in Genome Folding and Transcriptional Gene Regulation. *Annu. Rev. Genomics Hum. Genet.* **17**, 17-43.

Mihaly, J., Hogga, I., Gausz, J., Gyurkovics, H. and Karch, F. (1997). In situ dissection of the Fab-7 region of the bithorax complex into a chromatin domain boundary and a Polycomb-response element. *Development* **124**, 1809-1820.

Mihaly, J., Barges, S., Sipos, L., Maeda, R., Cleard, F., Hogga, I., Bender, W., Gyurkovics, H. and Karch, F. (2006). Dissecting the regulatory landscape of the Abd-B gene of the bithorax complex. *Development* **133**, 2983-2993.

Mohan, M., Bartkuhn, M., Herold, M., Philippen, A., Heinl, N., Bardenhagen, I., Leers, J., White, R. A. H., Renkawitz-Pohl, R., Saumweber, H. et al. (2007). The Drosophila insulator proteins CTCF and CP190 link enhancer blocking to body patterning. *EMBO J.* **26**, 4203-4214.

Moon, H., Filippova, G., Loukinov, D., Pugacheva, E., Chen, Q., Smith, S. T., Munhall, A., Grewe, B., Bartkuhn, M., Arnold, R. et al. (2005). CTCF is conserved from Drosophila to humans and confers enhancer blocking of the Fab-8 insulator. *EMBO Rep.* **6**, 165-170.

Page, A. R., Kovacs, A., Deak, P., Torok, T., Kiss, I., Dario, P., Bastos, C., Batista, P., Gomes, R., Ohkura, H., Russell, S. and Glover, D. M. (2005). Spotted-dick, a zinc-finger protein of *Drosophila* required for expression of *Orc4* and S phase. *EMBO J.* **24**, 4304-4315.

Perez-Lluch, S., Cuartero, S., Azorin, F. and Espinas, M. L. (2008). Characterization of new regulatory elements within the Drosophila bithorax complex. *Nucleic Acids Res.* **36**, 6926-6933.

Rao, S. S. P., Huntley, M. H., Durand, N. C., Stamenova, E. K., Bochkov, I. D., Robinson, J. T., Sanborn, A. L., Machol, I., Omer, A. D., Lander, E. S. et al. (2014). A 3D map of the human genome at kilobase resolution reveals principles of chromatin looping. *Cell* **159**, 1665-1680.

Schweinsberg, S. E. and Schedl, P. (2004). Developmental modulation of Fab-7 boundary function. *Development* **131**, 4743-4749.

Schweinsberg, S., Hagstrom, K., Gohl, D., Schedl, P., Kumar, R. P., Mishra, R. and Karch, F. (2004). The enhancer-blocking activity of the Fab-7 boundary from the Drosophila bithorax complex requires GAGA-factor-binding sites. *Genetics* **168**, 1371-1384.

Scott, K. C., Taubman, A. D. and Geyer, P. K. (1999). Enhancer blocking by the *Drosophila* gypsy insulator depends upon insulator anatomy and enhancer strength. *Genetics* **153**, 787-798.

Sexton, T., Yaffe, E., Kenigsberg, E., Bantignies, F., Leblanc, B., Hoichman, M., Parrinello, H., Tanay, A. and Cavalli, G. (2012). Three-dimensional folding and functional organization principles of the Drosophila genome. *Cell* **148**, 458-472.

Vogelmann, J., Le Gall, A., Dejardin, S., Allemand, F., Gamot, A., Labesse, G., Cuvier, O., Negre, N., Cohen-Gonsaud, M., Margeat, E. et al. (2014). Chromatin insulator factors involved in long-range DNA interactions and their role in the folding of the Drosophila genome. *PLoS Genet.* **10**, e1004544.

Wolle, D., Cleard, F., Aoki, T., Deshpande, G., Schedl, P. and Karch, F. (2015). Functional requirements for Fab-7 boundary activity in the bithorax complex. *Mol. Cell. Biol.* **35**, 3739-3752.

Zolotarev, N., Fedotova, A., Kyrchanova, O., Bonchuk, A., Penin, A. A., Lando, A. S., Eliseeva, I. A., Kulakovskiy, I. V., Maksimenko, O. and Georgiev, P. (2016a). Architectural proteins Pita, Zw5,and ZIPIC contain homodimerization domain and support specific long-range interactions in Drosophila. *Nucleic Acids Res.* **44**, 7228-7241.

Zolotarev, N. A., Maksimenko, O. G., Georgiev, P. G. and Bonchuk, A. N. (2016b). ZAD-domain is essential for nuclear localization of insulator proteins in Drosophila melanogaster. *Acta Naturae* **8**, 97-102.

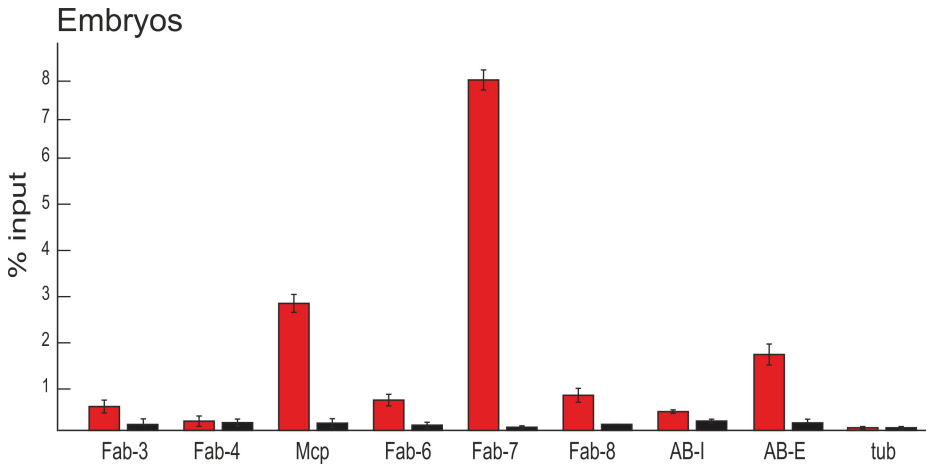

Fig. S1. Binding of Pita at the boundaries of BX-C in embryos. Chromatin was isolated from 12-24 h embryos and incubated with antibodies against Pita (red bars). Nonspecific IgG (black bars) was used as a negative control. The results of ChIPs are presented as percentages of input DNA. The γ*Tub37C* (tub) coding region, which is devoid of binding sites for Pita, was used as a negative control. Error bars indicate standard deviations of triplicate PCR measurements from three independent biological samples of chromatin.

Development • Supplementary information

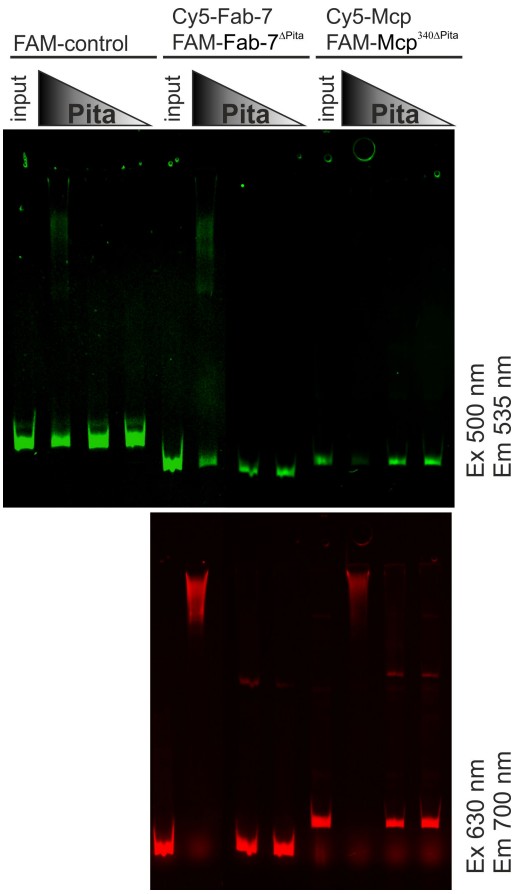

Fig. S2. EMSA of the Pita recombinant zinc finger domains with DNA fragments from the Fab7 and Mcp elements containing Pita binding sites which were used in the replacement experiments. Zinc finger domains of Pita fused with MBP were incubated with fluorescently labeled DNA fragments; *Fab7* and *Mcp* labeled with Cy5 (*wt*) and corresponding fragments with the mutated Pita binding sites labeled with FAM. Also, a heterologous fragment with no Pita binding sites labeled with FAM was used as a negative control for binding (marked as FAM-control). Signals were detected for the FAM-labeled fragment at the Ex 500 nm / Em 535 nm and for Cy5-labeled fragment at the Ex 630 nm / Em 700 nm. Specificity of interaction was demonstrated by incubation of DNA fragments with varying amounts of Pita protein presented as a series of 2-fold dilutions.

Development • Supplementary information

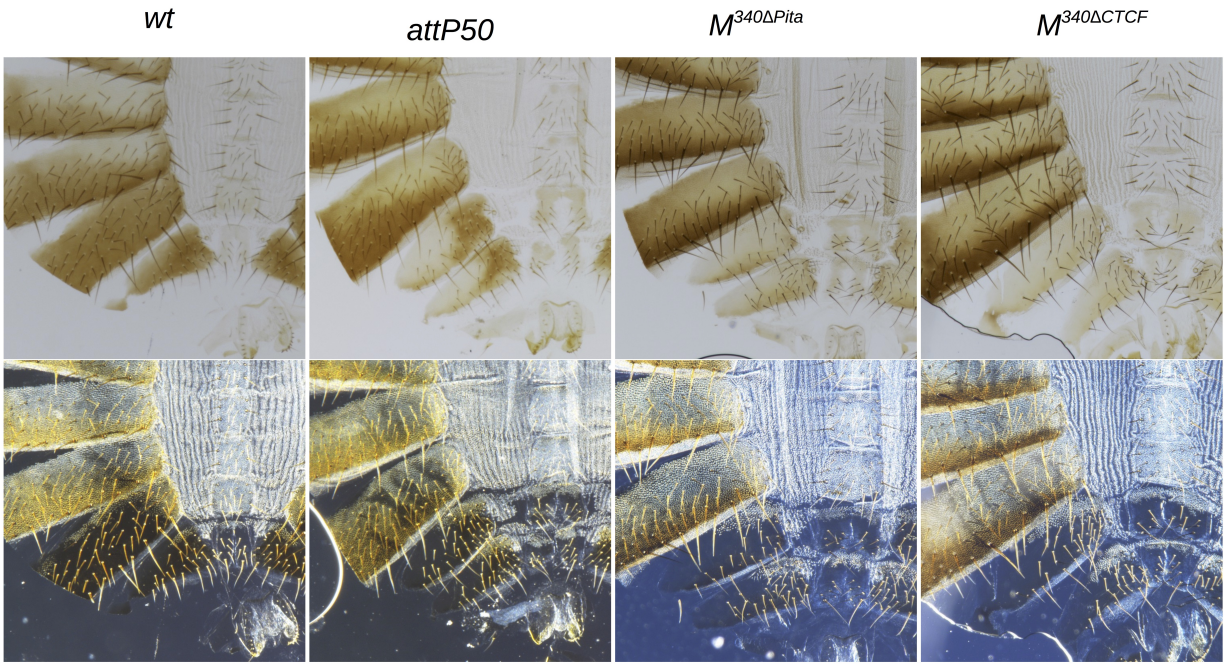

Fig. S3. Morphology of the abdominal segments of the M^{340} mutant females. In $M^{340\Delta Pita}$ and $M^{340\Delta CTCF}$ homozygous females A6 is completely transformed into A7 thus demonstrating a clear GOF transformation.

Development • Supplementary information

Fig. S4. Sequences of the substitution fragments. Complete sequences of all the substitution fragments along with the schematics of the positions of binding and mutation sites are shown.

Pita×5

(*Hind*III)*aagctt*gatctttagccaagacgcgaacccgaatccgaaactttagccaagacgcgaacccgaatccgaaactttagccaagacgcgaacccgaatccgaaacttagccaagacgcgaacccgaatccgaaactttagccaagacgcgaacccgaatccgaagatctaatatc*gaattc*(EcoRI)

Designations: *restriction sites*, Pita binding sites

Fab-7

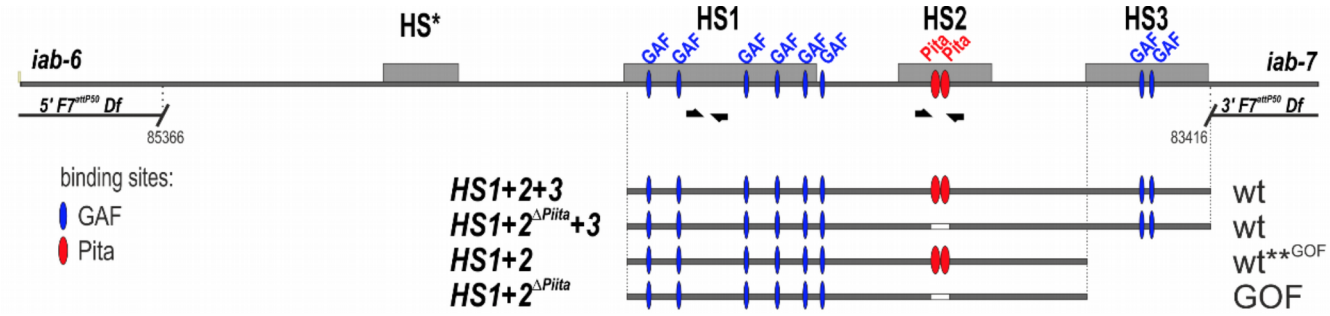

HS1+2+3

gatttcaagctgtgtggcgggggaagaggaagagagcggaaagtgcagcgcccaataagcaaatggcagctgtcacggggaagcacagagagt
gcagaaaggggaaaaaacattggggcatatcaacgcgccaaaaagaaaaacaaaaagagcgaggtagaatgtcgctcaaagagcgacacgtga
acaggtgcagtagtaaatataagcaaagagagttggaaagagtattggctaagagcgaccgctcactaacacatagataaattaagagagacgtga
taagagaaccgcacgcacaccaccgcaaaatccaattggaagagagcgactgcttgaatgtattggtaagcaagagagcggctaggtttgatggttt
gattggaattcagttgccgttcgaaatatttttgataaaatataaaaaattaattcagaggctgaggcaagtctaaaaacaatgctttgcctaagaatt
cgtagcttttataattttttttttaattttgaaattagcattttattttttaaatgattctccaattaagccaactggtttccaactctagcggtgaccctcacc
ttttggtttgcgtaccgactaagtccgagcagtgctgcgcatccctttgagccttagtatacccatctcgctcttagccacccctaaataccgttacttac
cctgggcaacttccttcgtccgtcggcctttgtttctgcatttttttttgtttttgtctgggcgacgacgcagtcgcagaaagtccctcgaaattcctccgctc
cctcgctcgctcacaatcctgtttttttgggcctctagtttttcggggccccgagtttcggtcgctcacgtcg

HS1+2ΔPita+3

Gatttcaagctgtgtggcgggggaagaggaagagagcggaaagtgcagcgcccaataagcaaatggcagctgtcacggggaagcacagagagt
gcagaaaggggaaaaaacattggggcatatcaacgcgccaaaaagaaaaacaaaaagagcgaggtagaatgtcgctcaaagagcgacacgtga
acaggtgcagtagtaaatataagcaaagagagttggaaagagtattggctaagagcgaccgctcactaacacatagataaattaagagagacgtga
taagagaaccgcacgcacaccaccgcaaaatccaattggaagagagcgactgcttgaatgtattggtaagcaagagagcggctaggtttgatggttt
gattggaattcagttgccgttcgaaatatttttgataaaatataaaaaattaattcagaggctgaggcaagtctaaaaacaatgctttgcctaagaatt
cgtagcttttataattttttttttaattttgaaattagcattttattttttaaatgattctccaattaagccaactggtttccaactctagcggtgac*atcgaat*
*tcgatt*aagtccgagcagtgctgcgcatccctttgagccttagtatacccatctcgctcttagccacccctaaataccgttacttaccctgggcaacttcc
ttcgtccgtcggcctttgtttctgcatttttttttgtttttgtctgggcgacgacgcagtcgcagaaagtccctcgaaattcctccgctccctcgctcgctcac
aatcctgtttttttgggcctctagtttttcggggccccgagtttcggtcgctcacgtcg

Development • Supplementary information

HS1+2 and HS1+2ΔPita was amplified without HS3 (*iab-7* PRE)

Designations: F7 HS1+2, GAF binding sites, Pita binding sites, *mutated sequence*, HS3 (*iab-7* PRE)

gtgagtggcgagcagagcagcatggagcgagcatggccgctgtggaataccgcactgtcgtaggcacgagcgcgagcgagagaggccaagagcac

caagaacttcacaacagacgacgtcgcag

gctctctttcacatccatgatggctgccgctgtctcgcctcttcttcttcattttcagctcggccatcatggggctccattaaatccactgcctcttcgccgg

gaatccgaattgccgacat

agagcagcatggagcgagcatggccgctgtggaataccgcactgtcgtaggcacgagcgcgagcgagagaggccaagagcacgctctctttcacat

caagaacttcacaacagacgacgtcgcaggtgagtggcgagc

ccatgatggctgccgctgtctcgcctcttcttcttcattttcagctcggccatcatggggctccattaaatccactgcctcttcgccgggaatccgaattgc

cgacat

Mcp

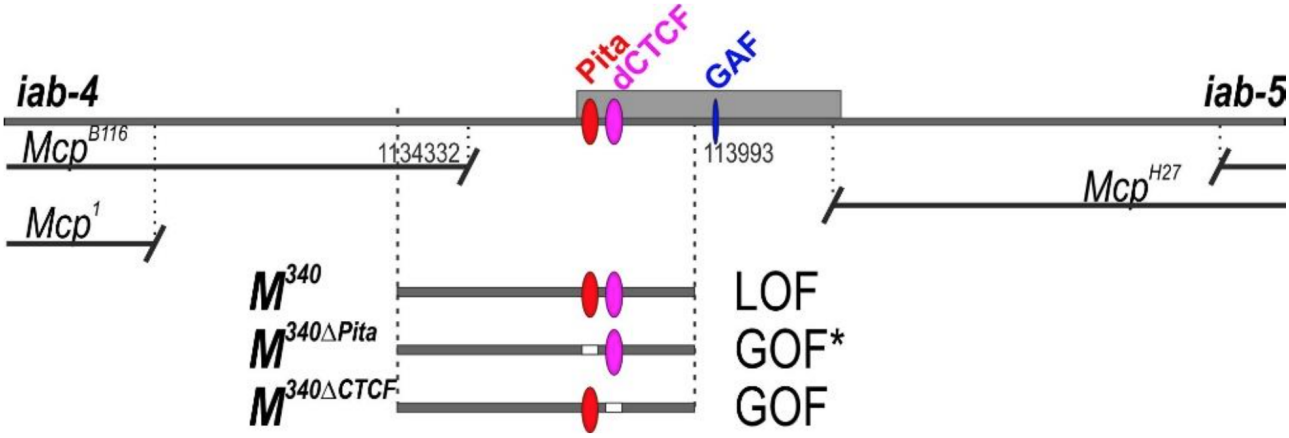

M340

gctcagagtacataagcgacgcccaaaaagcccaaatgtagagctttttcgaaattaaacagaaagtcgggtctgcaaataagggcttttctgggga
agaaataaattatatcttaataaatatattttaaacttaactcagacttggatttattttgaactacacacttaagtgatttaaataattttaaatatattt
cttacataaatt**tagccaatatccaaacct**ttttgcgct**ggcgccccctattgtttttc**tttcgcagctcatgctttgctggcaacccaccagaggacgct
cgctgattgaatcgcattacgcacacttacaacgattggg

M340 ΔPita

Gctcagagtacataagcgacgcccaaaaagcccaaatgtagagctttttcgaaattaaacagaaagtcgggtctgcaaataagggcttttctgggga
agaaataaattatatcttaataaatatattttaaacttaactcagacttggatttattttgaactacacacttaagtgatttaaataattttaaatatattt
cttacataaatt*gaattct*ttgcgct**ggcgccccctattgtttttc**tttcgcagctcatgctttgctggcaacccaccagaggacgctcgctgattgaatcg
cattacgcacacttacaacgattggg

M340 ΔCTCF

Development • Supplementary information

gctcagagtacataagcgacgcccaaaaagcccaaatgtagagctttttcgaaattaaacagaaagtcgggtctgcaaataagggcttttctgggga
agaaataaattatatcttaataaatatattttaaacttaactcagacttggatttattttgaactacacacttaagtgatttaaataattttaaatatattt
cttacataaatt**tagccaatatccaaacct***gaattct***c**tttcgcagctcatgctttgctggcaacccaccagaggacgctcgctgattgaatcgcattac
gcacacttacaacgattggg

Designations: **Pita binding sites**, **CTCF binding sites,** *mutated sequence*,

Development • Supplementary information

Mcp$^{340\Delta CTCF}$ male

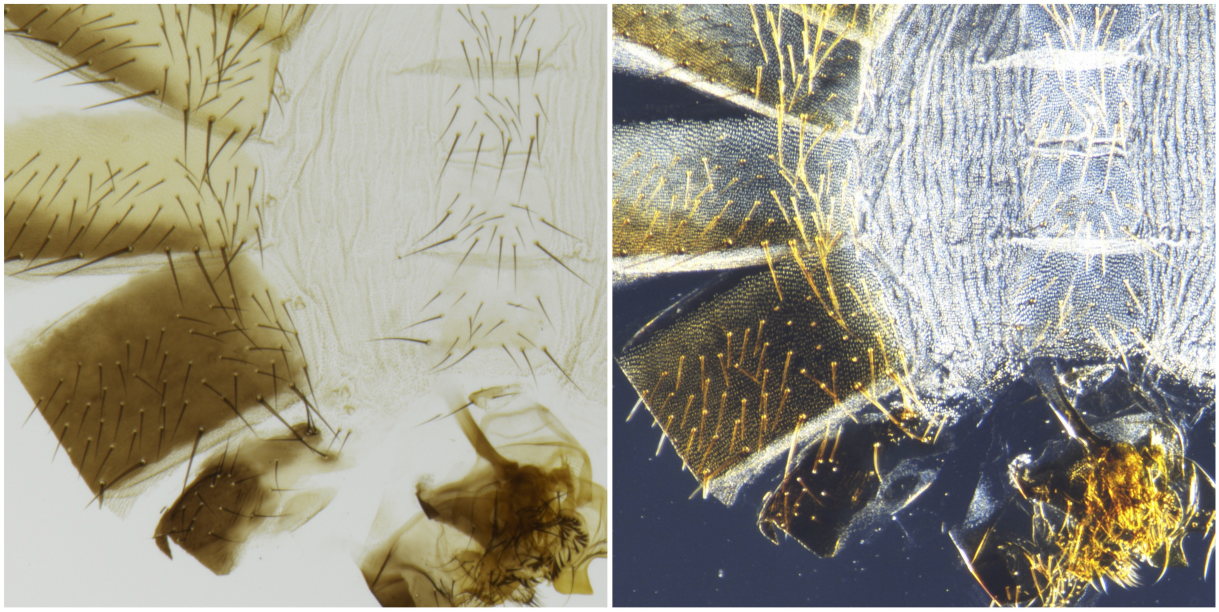

Fig. S5. Morphology of the abdominal segments of the *M*$^{340\Delta CTCF}$ mutant males. About 10% of males of this genotype demonstrate a larger remnant of the A6 tergite, with a mixture of the GOF, LOF, and features resembling wild type: only a part of the tergite surface is covered in trichome hairs, while the rest of the surface is devoid of trichomes, like in a wild type A6 tergite.

Development • Supplementary information

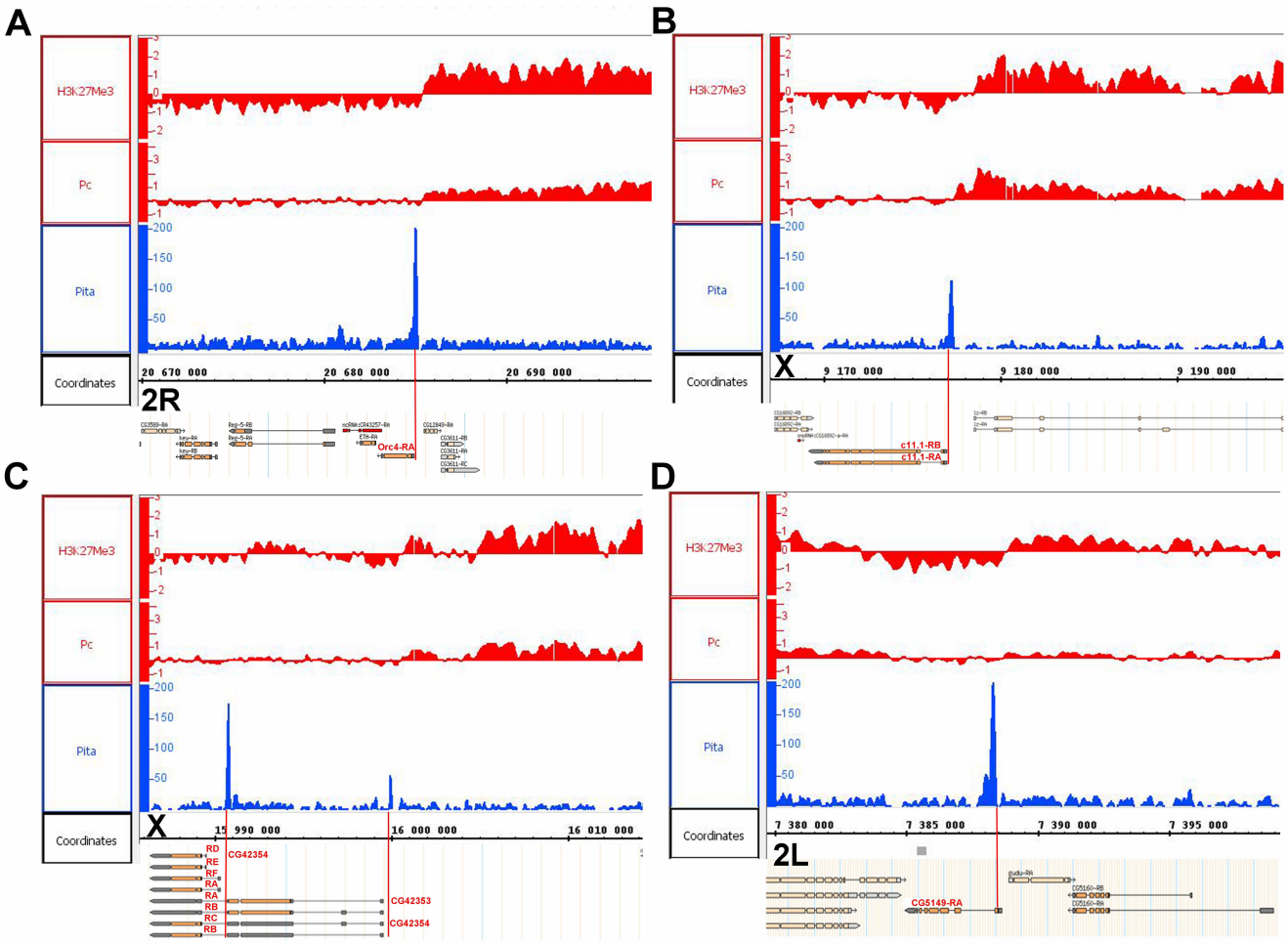

Fig. S6. Chromosomal landscapes at the gene promoters with the Pita binding sites.

Coverage vectors for Pita (blue track) (UCSC dm3 *Drosophila melanogaster* genome assembly) at the gene promoters with a ChIP-chip tracks for the Polycomb and H3K27me3 (red tracks) binding profiles (downloaded from ModEncode). Coordinates and genes are presented under the coverage histograms: **A.** *Orc4*, **B.** *c11.1*, **C.** *CG9216* a.k.a *CG42353* and *CG42354*, **D.** *CG5149*. Red vertical lines mark coincidences of Pita peaks and gene promoters.

Development • Supplementary information

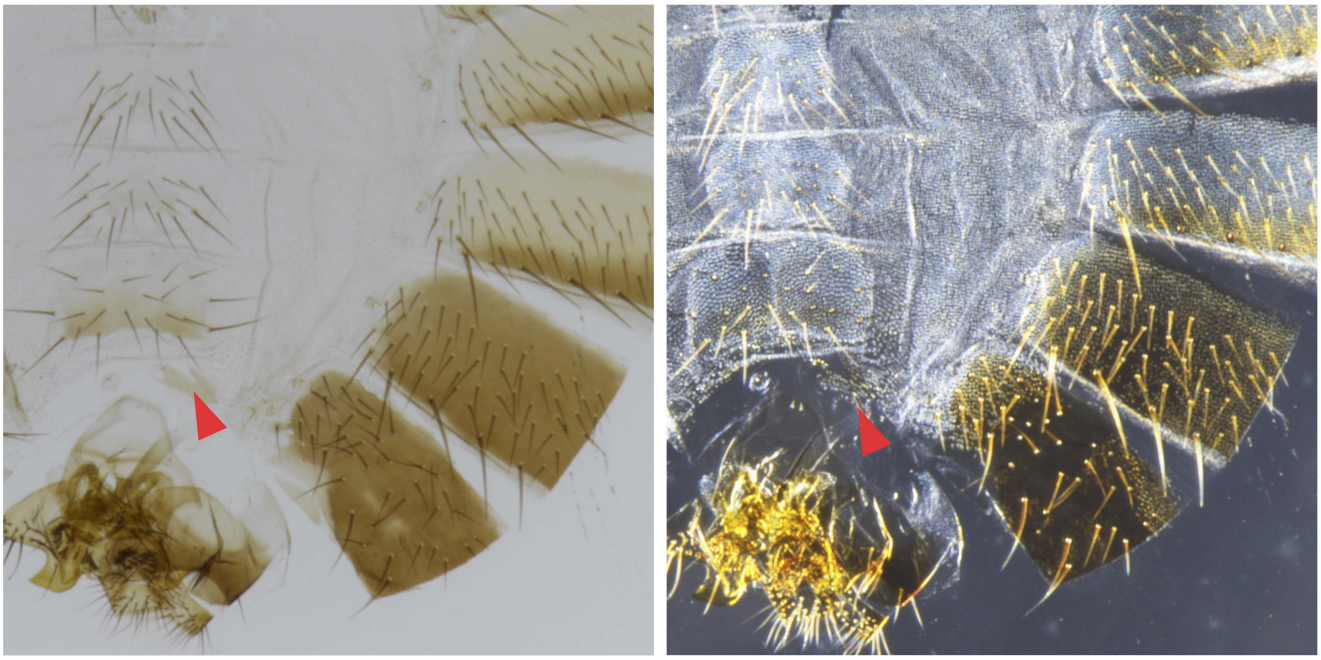

Fig. S7. Morphology of the abdominal segments in some of the *HS1+2* mutant males. Though the vast majority of *HS1+2* males lack an A6 sternite, infrequently (~10%) we observe a remaining small patch of sternite tissue (red arrow), which is even more clearly seen in the dark field as a lawn of trichomes.

Development • Supplementary information

Table S1. The list of oligonucleotides used in the study.

Primer	Sequence (5'---->3')
CHIP analysis	
γTub37C_d	GCTTTCCCAAGAAGCTCATACA
γTub37C_r	GGTTCAGTGCGGTATTATCCAG
RpL32_d	GTTCGATCCGTAACCGATGT
RpL32_r	CCAGTCGGATCGATATGCTAA
hsp70_d	GACAGAGTGAGAGAGCATTAG
hsp70_r	GGTTATTGTGGTAGGTCATTTG
FAB3_d	TAAAGGCCAATGCACAAAGGCGAC
FAB3_r	ACGCTTCAGCGAACGGAATACAGA
FAB4_d	CAATTTGCCAATATTTCGCAGTCCCT
FAB4_r	CCCTGGCGGGCATATGAGAAA
MCP_d	CGCGGCCATGTATTATGT
MCP_r	TACAACGCTTGGGTTTCTC
FAB6_d	CTGCCCAGTGGGAGATACAAAGAT
FAB6_r	AGCTAAACCCGATTTGCTTTGCCG
FAB7_d (=HS2_d)	TAAGCCAACTGGTTTCCAACTCT
FAB7_r (=HS2_r)	TTGCCCAGGGTAAGTAACGGTAT
FAB8_d	TGTTGGTGAGCAAGCGAAGA
FAB8_r	CGAACATTTTTTACGCGACATGT
AB-I_d	CCAACAACAAGCCAACTAACTACA
AB-I_r	ACGAACAAAAAACGCTCTCAGAC
HS1_d	CGAGGTAGAATGTCGCTCAAAG
HS1_r	GCGTGCGGTTCTCTTATCAC
i7_d	GTCGCAAGAACTTCACAACAG
i7_r	GCCATCATGGATGTGAAAGA
FUB_d	TCAGCAATTGTCAGGTGTCC
FUB_r	CATGAGCGAGTCCTTGTGAA
FUB2_d	AATTTCGTGTTCGCACTTCC
FUB2_r	GGCAGCACTAGCGTCAAAA
100C_d	CGACAGCATGTAACAGGTATAA
100C_r	CCCGAGGTTTCAACTTTCATA
Primers for EMSA	
EMSA_F_d	FAM-CTCACTATAGGGCGAATTG
EMSA_F_r	FAM-CGCCAAGCTCGAAATTA
EMSA_C_d	Cy5-CTCACTATAGGGCGAATTG
EMSA_C_r	Cy5-CGCCAAGCTCGAAATTA

Development • Supplementary information